Journal of Materials Chemistry A

Accepted Manuscript

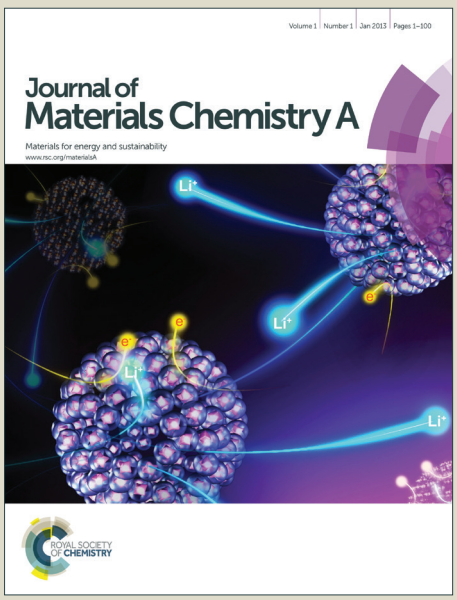

ROYAL SOCIETY OF CHEMISTRY

www.rsc.org/materialsA

Journal Name

ARTICLE

Direct amination of Si nanoparticles for the preparation of Si @ ultrathin SiO_x @ graphene nanosheets as high performance lithium-ion battery anodes†

Received 00th January 20xx,
Accepted 00th January 20xx

DOI: 10.1039/x0xx00000x

www.rsc.org/

Jin Niu, Su Zhang, Yue Niu, Huaihe Song*, Xiaohong Chen, Jisheng Zhou and Bin Cao

NH_2-termitated Si nanoparticles with an ultrathin silica shell have been efficiently obtained by one-step reaction in ammonia-water-ethanol solution. Graphene nanosheets encapsulated Si @ ultrathin SiO_x have been fabricated by self-assembly and thermal treatment. Because of the uniform utrathin SiO_x shell and superior GNSs encapsulation structure, this material shows a reversible capacity of 2391.3 mAh g^{-1}, maintaining 1844.9 mAh g^{-1} after 50 cycles at the current density of 200 mA g^{-1}, and good rate and long cycle performance (~700 mAh g^{-1} at 2000 mA g^{-1} after 350 cycles) as well.

1 Introduction

Si is one of the most promising high-capacity anode materials for Lithium-ion batteries (LIBs). It has the highest theoretical specific capacity (4200 mAh g^{-1}) which is 10 times higher than that of graphite.[1, 2] But severe volume change(>300%) during lithiation/delithiation results in the structural destruction, and further leads to the loss of electrical contact between active materials themselves or active materials and the current collectors.[3-5] Moreover, new solid electrolyte interphase (SEI) continuously forms on the new surface of Si. All of these problems cause the poor cycling and rate performance for Si-based anode materials.[6-9]

Recent studies have shown that the internal stress of Si induced during lithiation can be accommodated by using special nanostructured Si including nanoparticles,[10, 11] nanofilms,[12, 13] nanowires,[2, 14] nanotubes,[15, 16] hollow spheres[17, 18] and porous Si[19-22]. However, designing of novel nanostructures cannot overcome the issue of unstable SEI. One attractive strategy to stablize the SEI is to encapsulate Si nanostructures with self-supporting and void-containing carbon. Some advanced matrices have been presented, such as Si yolk-carbon shell,[23, 24] Si nanowire core-void-carbon shell[25] and Si core-nanoporous carbon shell[26]. Encapsulation of Si nanoparticles by graphene nanosheets (GNSs) is another way with obvious advantages: flexible GNSs coatings can enhance the conductivity of the electrode materials and accommodate large volume change of the Si nanoparticles, and avoiding direct contact between the electrolyte and Si can prevent the continuous deposition of SEI.[9, 27-30]

Simply mixing graphene oxide (GO) and Si nanoparticles in water and further treated by thermal annealing is a common route to synthesize Si nanoparticles-graphene nanosheets composites (Si-GNSs).[31-33] However, Si nanoparticles are not well encapsulated by GNSs because of their poor dispersability in water and very weak interaction between Si nanoparticles and GNSs. Self-assembly through electrostatic interaction (or covalent interaction) is an efficient route to obtain good encapsulation structure and enhance the synergistic effect between modified material and GNSs.[34-36] GO is naturally negatively charged when dispersed in water.[37,38] When electropositive surface property is achieved by modification, Si nanoparticles can not only well dispersed in water but also well encapsulated by graphene oxide[39-42] with opposite charges through electrostatic interaction. However, pretreatment must be taken to modify the inert surface of Si.[29, 43-45] Typically, Zhu et al. used Piranha solution (H_2SO_4/H_2O_2) to activate the surface of Si nanowires, then rendered the treated Si nanowires positively charged by aminopropyltriethoxysilane (APTES) in toluene for 24 h.[29] Sun et al. used hydrochloride solution (37%) to hydroxylate Si nanoparticles and then aminated them in dry toluene at 110 °C for 24h.[45] In other works, Si nanoparticles with a native oxide layer because of oxidization in air are employed for modification. These pretreatments, however, are not only hard to control but environmental-unfriendly as well. Moreover, the treatments will also cause formation of silica shell (2 nm-7 nm) on Si surface; and the silica shell limits the electrochemical activity and reduces the specific capacity of electrode material.[39] Therefore, additional HF etching is required to remove the silica shell.[29, 39] Instead of using Si nanoparticles with an oxide layer, Li et al. used diazonium functionalized Si nanoparticles in their work and then modified the functionalized Si by situ polymerization of aniline on the surface. The PANI-grafted Si nanoparticles can be wrapped by

State Key Laboratory of Chemical Resource Engineering, Beijing Key Laboratory of Electrochemical Process and Technology for Materials, Beijing University of Chemical Technology, Beijing, 100029, P. R. China. Fax: (+86) 10-6443-4916; Tel: (+86) 10-6443-4916; E-mail: songhh@mail.buct.edu.cn

†Electronic Supplementary Information (ESI) available. See DOI: 10.1039/x0xx00000x

Journal Name

ARTICLE

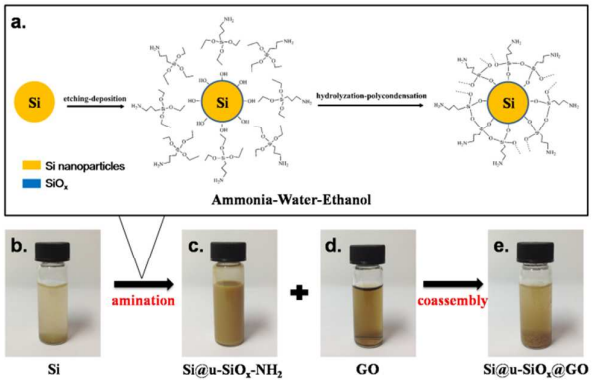

Fig. 1 (a) Schematic description for the amination of Si nanoparticles; photographic images of (b) Si nanoparticles, (c) Si@u-SiO_x-NH_2, (d) GO and (e) Si@u-SiO_x@GO in water.

GO via π-π interaction and electrostatic attraction.[41] Ye et al. modified Si nanoparticles with benzoyl acid. The Si-COOH can self-assembly with positively charged graphene (graphene-modified protic ionic liquid) through electrostatic attraction.[42]

Herein, we presented a new route to fabricate GNSs encapsulated Si nanoparticles. Firstly, NH_2-termitated ultrathin silica shell/Si core nanoparticles (Si@u-SiO_x-NH_2) were directly obtained by grafting amino silane on the surface of the Si nanoparticles in ammonia-water-ethanol solution through etching-deposition and simultaneous hydrolyzation-polycondensation process (Fig. 1). Si nanoparticles can be easily hydroxylated by this weakly alkaline solution (molarity of ammonia is ~0.2M) through etching-deposition process.[46] The alkaline solution here not only plays as an etching agent but also a catalyst[47] so that APTES can be grafted on Si nanoparticles in a short time. Then, Si@u-SiO_x@GNSs were obtained by self-assembly in water solution and further thermal reduction. Due to the thinner SiO_x on the Si nanoparticles and fine GNSs encapsulation structure, Si@u-SiO_x@GNSs exhibit higher specific capacity and better rate performance than GNSs encapsulated Si nanoparticles with thick SiO_x shell (Si@t-SiO_x@GNSs). What's more, no additional toxic reagents and extra energy were needed in this route. We provided an environment-friendly approach to preparation of high performance Si-GNSs anode materials for LIBs.

2 Experimental Section

2.1 Sample Preparation

Preparation of Si@u-SiO_x-NH_2. To prepare Si@u-SiO_x-NH_2, 100 mg of the Si nanoparticles powder (Shanghai ST-Nano Science & Technology Co., Ltd; Particle size: 20-160 nm) were firstly dispersed in to 120 ml of ethanol by water bath sonication. Subsequently, 2 ml of the concentrated ammonia solution (14.5 M) and 10 ml of water was slowly added into the dispersion and then 0.1 ml of APTES was added immediately. The reaction was carried out at room temperature with magnetic stirring. After 1 h, Si@u-SiO_x-NH_2 were separated by centrifugation, removing ammonia and unreacted APTES using ethanol, and dried at 40 °C.

Preparation of Si@t-SiO_x-NH_2. We used two-step method to prepare Si@t-SiO_x-NH_2. (1) 100 mg of the Si nanoparticles powder were firstly dispersed in to 120 ml of ethanol by water bath sonication. Subsequently, 2 ml of the concentrated ammonia solution (14.5 M) and 10 ml of water was slowly added into the dispersion. The reaction was carried out at room temperature with magnetic stirring. After 1 h, Si nanoparticles with thick SiO_x shell (Si@t-SiO_x) were obtained through an etching-deposition process[46] and then separated by centrifugation, removing ammonia using ethanol, and dried at 40 °C. (2) As-prepared Si@t-SiO_x were dispersed into 50 ml of water by sonication, followed by adding 0.1 ml of APTES into the dispersion. The reaction was also carried out at room temperature with magnetic stirring. After 24 h, the Si@t-SiO_x-NH_2 were obtained through a hydrolytic polycondensation process and then separated by centrifugation, removing unreacted APTES using ethanol, and dried at 40 °C.

Preparation of GO. GO was prepared from natural graphite by a modified Hummers'method.[48,49] The obtained GO was diluted with water and centrifugated at 4000 rpm for 20 min to remove the unexfoliated GO, and then dried by vacuum freeze-drying.

Preparation of Si@u-SiO_x@GNSs, Si@t-SiO_x@GNSs and Si/GNSs. To prepare Si@u-SiO_x@GNSs and Si@t-SiO_x@GNSs. 80 mg GO was dispersed in 400ml water by ultrasonic treatment. 80 mg Si@u-SiO_x-NH_2 or Si@t-SiO_x-NH_2 were also dispersed in 400 ml

water and then slowly dropped into the diluted GO aqueous solution. After 0.5 h, the precipitates were freeze dried, followed by reduction at 750 °C for 2 h under Ar atmosphere to obtain Si@u-SiO_x@GNSs or Si@t-SiO_x@GNSs (heating rate 2 °C min^{-1}). Si nanoparticles/graphene nanosheets composites (Si/GNSs) were prepared by simply mixing of Si nanoparticles and GO aqueous solution, being dried and reduced under the same conditions.

2.2 Characterizations and Electrochemical Measurements

The obtained samples were characterized by X-ray diffraction (XRD, Rigaku D/max-2500B2+/PCX, Cu Kα, λ=1.54056 Å), scanning electron microscopy (SEM, ZEISS SUPRATM 55), transmission electron microscopy (TEM, HT-800, Hitachi), high resolution transmission electron microscopy (HRTEM, JEOL 3010, JEOL), thermogravimetric analysis (TGA, STA449 Jupiter, NETZSCH from room temperature to 750 °C at a heating rate of 10 °C min^{-1} in air ambience) and X-ray photoelectron spectroscopy (XPS, ESCALAB 250 with monochromatic Al K X-ray sources of 30 eV pass energy in 0.5 eV step over an area of 650 μm × 650 μm). Zeta potential measurements were performed using a Zetasizer Nano Series (Malvern, samples were dispersed in water with a concentration of 0.2 mg ml^{-1}).

The electrochemical measurements were tested with CR2032 coin-type cell. For preparing working electrodes, active sample, PolyVinylidene DiFluoride (PVDF) or sodium alginate (SA) and acetylene black at a weight ratio of 80 : 10 : 10 were coated on the circular foam nickel plates (the area of nickel plate is ~1.54 cm^2, the loading weight of active material is 2-3 mg for each plate). 1 M $LiPF_6$ solution in the mixture of ethylene carbonate, diethyl carbonate and fluoroethylene carbonate (v/v/v, 1:1:0.05) was employed as electrolyte. After assembling, the cells were charged and discharged in Land CT2001A system at various current densities in the voltage range from 0.01 to 2.5 V. The cyclic voltammetry and electrochemical impedance spectral (EIS) measurements were carried out on a ZENNIUM (Zahner) electrochemical working station. For the cyclic voltammetric measurements, the sweep rate was 0.1 mV s^{-1} and the potential range was 0.01 to 2.5 V. For the EIS measurements, the frequency range was from 100 kHz to 10 mHz.

3 Results and Discussion

The preparation method of Si@t-SiO_x were similar to the reported one by our group[46], Si@t-SiO_x with plenty of hydroxyl

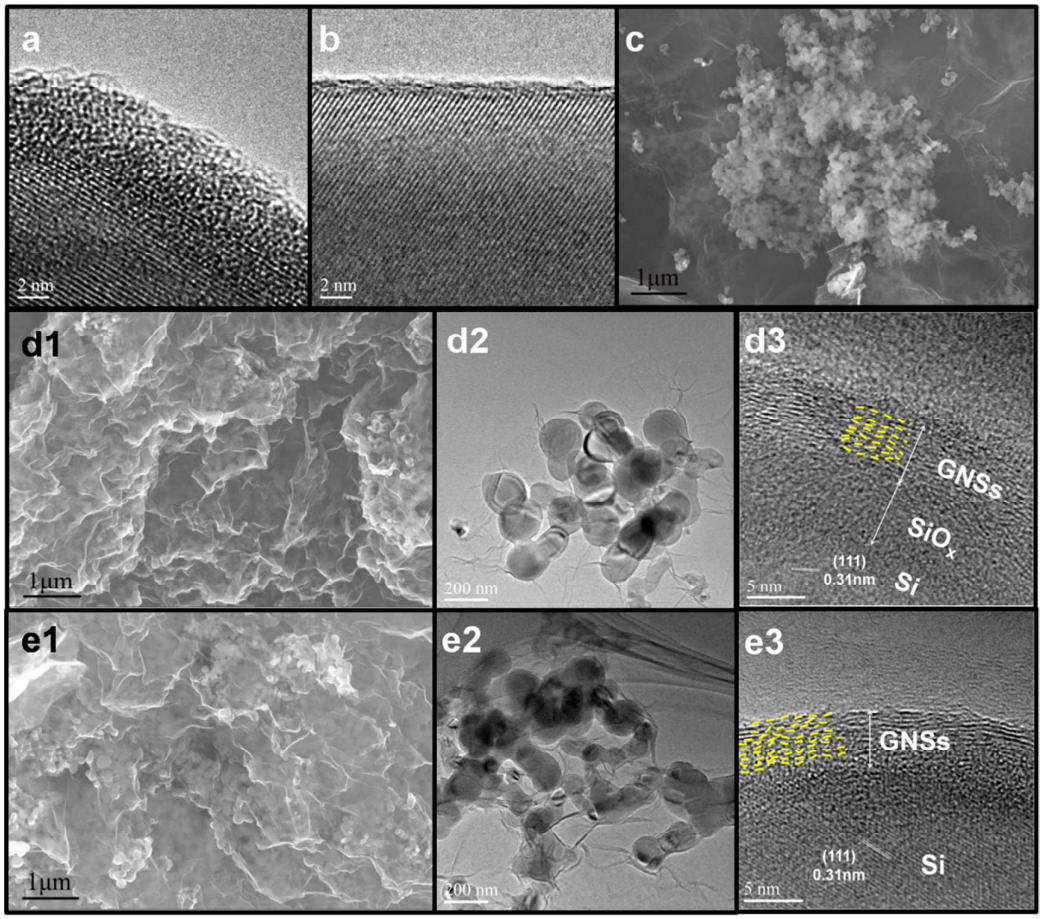

Fig. 2 (a) HRTEM image of Si@t-SiO_x, (b) HRTEM image of Si@u-SiO_x-NH_2, (c) SEM image of Si/GNSs; (d1) SEM, (d2) TEM and (d3)HRTEM images of Si@t-SiO_x@GNSs; (e1) SEM, (e2) TEM and (e3)HRTEM images of Si@u-SiO_x@GNSs.

Journal Name

ARTICLE

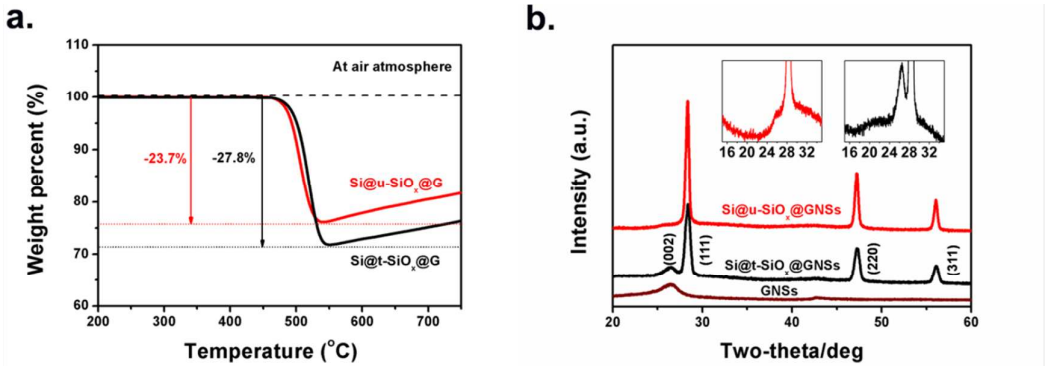

Fig. 3 (a) TGA curves of Si@u-SiO_x@GNSs and Si@t-SiO_x@GNSs; (b) XRD patterns of the Si@u-SiO_x@GNSs, Si@t-SiO_x@GNSs and GNSs.

were obtained through a continuously etching-deposition process, the thickness of the silica shell could be controlled as 3-5 nm (Fig. 2a). For Si@u-SiO_x-NH_2, however, when APTES was added into this system, rapid hydrolysis and uniform grafting of the APTES on newly formed silica shell protected the Si core from further etching, resulting in the formation of ultrathin NH_2-terminated silica shells with the thickness less than 1 nm (Fig. 2b) which was almost unchanged even the reaction time extends to 24h (Fig. S1). Zeta potential analysis was used to examine the surface modification effects of Si nanoparticles. The zeta potential of Si@t-SiO_x, Si@u-SiO_x-NH_2 and Si@t-SiO_x-NH_2 are -32.2 mV, 46.8 mV and 37.0 mV, respectively. All of them can be well dispersed in water. Because positively charged Si@u-SiO_x-NH_2 or Si@t-SiO_x-NH_2 are successfully obtained in ammonia-water-ethanol solution using APTES, Self-assembly can take place when they are mixed with the negatively charged GO (zeta potential: -55.4 mV) in water.[29, 35] The precipitates (Fig. 1e) were freeze-dried, followed by a thermal reduction at 750 °C to obtain Si@u-SiO_x@GNSs or Si@t-SiO_x@GNSs. Si/GNSs were also synthesized by simply mixing of Si nanoparticles and GO, being dried and reduced under the same conditions. From the SEM image of Si/GNSs, we can see that some of the Si nanoparticles are exposed without GNSs cover (Fig. 2c). But for Si@t-SiO_x@GNSs (Fig. 2d1 and 2d2) and Si@u-SiO_x@GNSs (Fig. 2e1 and 2e2), almost all of the nanoparticles are well encapsulated by crumpled GNSs. The difference of the SiO_x coatings can also be seen from the HRTEM images of Si@t-SiO_x@GNSs (Fig. 2d3) and Si@u-SiO_x@GNSs (Fig. 2e3) and the thickness of the GNSs shell (7-8 graphene layers) is ~5 nm. All these indicate that effective self-assembly is achieved by surface modified Si nanoparticles.

Fig. 3a shows the TGA curves of Si@u-SiO_x@GNSs and Si@t-SiO_x@GNSs. The weight loss recorded at ~550°C is due to the combustion of GNSs shells in air[50] and the gradually regained mass above 550°C is attributed to the oxidation of Si nanoparticles.[43] Therefore, the percentages of GNSs in Si@u-SiO_x@GNSs and Si@t-SiO_x@GNSs are calculated as 23.7% and 27.8%, respectively. Fig. 3b shows the X-ray diffraction (XRD) patterns of Si@u-SiO_x@GNSs, Si@t-SiO_x@GNSs and GNSs. For Si@u-SiO_x@GNSs and Si@t-SiO_x@GNSs, the peaks at around 28.5°, 47.2°, 56° correspond to the characteristic diffraction of Si. The peak at around 26° which can also be seen from the patterns of GNSs confirms the existence of GNSs in both Si@u-SiO_x@GNSs and Si@t-SiO_x@GNSs and the different diffraction intensity of this peak can be explained by the different GNSs and Si content in these two composites. Besides, a broad and weak diffraction peak at ~20° is only observed from the pattern of Si@t-SiO_x@GNSs which is the characteristic peak of SiO_x.[51]

The survey XPS spectra of Si nanoparticles, Si@u-SiO_x-NH_2 and Si@t-SiO_x-NH_2 are shown in Fig. 4. The Si 2p spectra of Si nanoparticles and Si@u-SiO_x-NH_2 show distinct peaks centered at 98.4 eV. However, no peak can be observed here for Si@t-SiO_x-NH_2. As we know, the XPS surface analysis depth is ~2 nm. This indicates that the thickness of SiO_x shell in the Si@u-SiO_x-NH_2 is less than 2 nm, which is thinner than that of the Si@t-SiO_x-NH_2. Moreover, the Si@t-SiO_x-NH_2 has a wider and stronger peak at 130.0 eV than that of the Si@u-SiO_x-NH_2. This peak is ascribed to SiO_x (Fig. 4a), indicating the formation of thicker SiO_x shell in Si@t-SiO_x-NH_2 than that of the Si@u-SiO_x-NH_2. Obvious N 1s peaks in spectra of Si@u-SiO_x-NH_2 and Si@t-SiO_x-NH_2 indicate the effective grafting of APTES with reactive silica shells (Fig. 4b1). The core level peaks can be split into two components (Fig. 4b2 and 4b3): signals at 399.5 eV correspond to amino originated from APTES, and signals at 401.4 eV are assigned to hydrogen-bonded amino or

Journal Name

ARTICLE

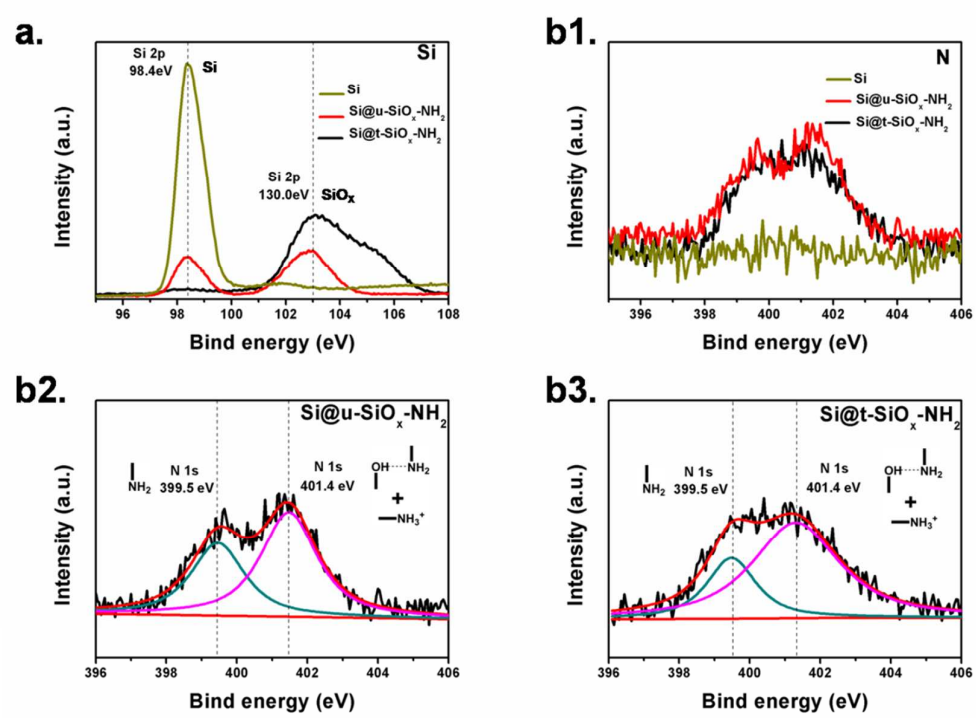

Fig. 4 (a) XPS Si 2p spectra of Si nanoparticles, Si@u-SiO_x-NH_2 and Si@t-SiO_x-NH_2; (b1) XPS N 1s spectra of (b2) Si@u-SiO_x-NH_2 and (b3) Si@t-SiO_x-NH_2.

protonated amino, also suggesting that we successfully grafted APTES on the surface of Si nanoparticles.[52]

Fig. 5a shows first three cyclic voltammetry (CV) curves of Si@u-SiO_x@GNSs. The first discharge process shows a sharp reduction peak at 0.05V, corresponding to the insertion of lithium ions into crystalline Si. In the subsequent cycles, a cathodic peak at 0.21V gradually evolves, resulting from the higher-voltage lithiation of amorphous Si[53]. The enhancement of this peak with increase of the scan times can be attributed to the activation process during the insertion/extraction.[53,54] Moreover, this appeared peak of Si@u-SiO_x@ GNSs in the second cycle becomes stronger than those of Si@t-SiO_x@ GNSs and Si/GNSs (Fig. S2a and S2b), suggesting that the Li extraction kinetics of former is better than those of latter two. The anodic part displays two peaks, at 0.31V and 0.5V, which can be attributed to the de-alloying of the Li-Si alloys. The results are consistent with the previous reports.[38, 39] The cycling stabilities of Si nanoparticles, Si/GNSs, Si@u-SiO_x@GNSs and Si@t-SiO_x@GNSs during charge-discharge between 0.01V-2.5V vs Li/Li^+ at the current density of 200 mA g^{-1} are shown in Fig. 5c and 5d**.** All the specific capacity is calculated based on the total mass of Si nanoparticles and GNSs. The initial discharge capacity of Si/GNSs is only 1350.4 mAh g^{-1} and capacity fading to 519 mAh g^{-1} after 50 cycles with a capacity retention ratio of 38.4%. The Si@t-SiO_x@GNSs show an initial discharge capacity of 1186.2 mAh g^{-1} but a high reversible capacity of 1092.2 mAh g^{-1} even after 50 cycles. Si@u-SiO_x@GNSs show the best capacitive and cyclic performance of all. The first discharge capacity of Si@u-SiO_x@GNSs is 2933.1 mAh g^{-1} with a high initial coulombic efficiency of 81.5% (Fig. 5b and 5c). The first charge capacity is as high as 2391.3 mAh g^{-1} and the capacitance retention is 1844.9 mAh g^{-1} after 50 cycles (77.2% of the first cycle capacity). After the first few cycles, the Coulombic efficiency is increased and stabilizes over 98%.

The large difference of cycle performance can be explained by their different structures and electrochemical mechanisms. The bad performance of Si/GNSs is attributed to that unmodified Si nanoparticles cannot be well encapsulated by GNSs because of the poor dispersibility in water and the weak interaction between Si nanoparticles and GO; For Si@t-SiO_x@GNSs and Si@u-SiO_x@GNSs, different thickness of SiO_x results in the different cycle performance, which can be explained essentially by the electrochemical mechanisms of Si

Journal Name

ARTICLE

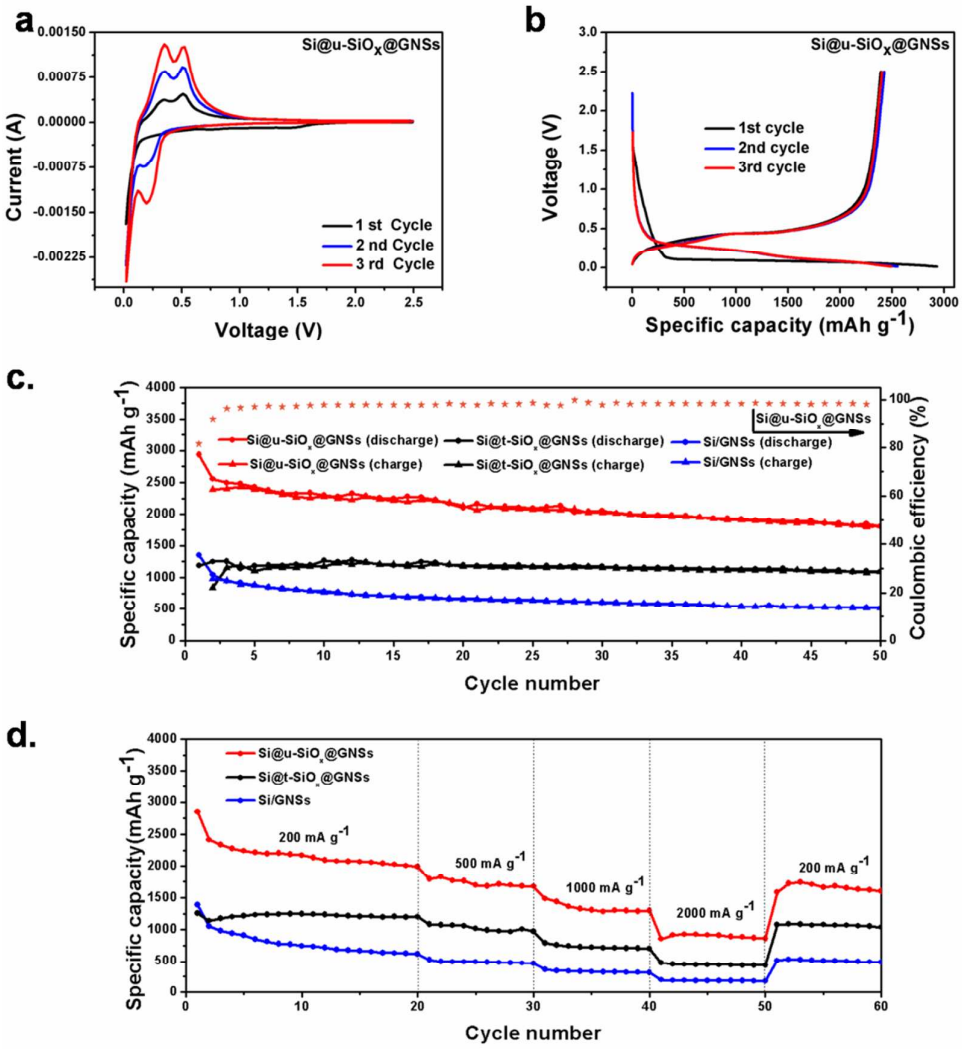

Fig. 5 (a) CV curves and (b) charge-discharge processes of Si@u-SiO_x@GNSs as anode materials for LIBs; (c) Cycling performance of Si@u-SiO_x@GNSs, Si@t-SiO_x@GNSs and Si/GNSs at the current density of 200 mA g^{-1} and (d) Rate capabilities.

and SiO_x. As shown in Equation (1), the charge-discharge process of Si can happen by direct delithiation and lithiation. At ambient temperature, maximum of x is 3.75 and the corresponding maximum theoretical specific capacity is 3579 mAh g^{-1}.[53] For SiO_x, however, the electrochemical mechanism is very complex. As show in Equation (2-4),[55] lithium ions firstly insert into Si to form Li_xO, lithium silicate and Si. Then produced Si subsequently react with lithium ions according to the Equation (1). The lithium silicate are mainly Li_4SiO_4[56,57] and $Li_2Si_2O_5$[58,59]. Li_xO and lithium silicate can buffer the volume expansion of Si[60,61] so Si@t-SiO_x@GNSs show better stability than Si@u-SiO_x@GNSs. However, the formations of Li_xO and Li_4SiO_4 are irreversible, resulting in low reversible capacity.[62] What is worse, Li_xO and lithium silicate are ionically poor conductor and decrease the cycle performance and rate capability.[63] Therefore, Si@u-SiO_x@GNSs show much higher reversible capacity than Si@t-SiO_x@GNSs.

$$Si + xLi^+ + xe^- \rightleftharpoons Li_xSi \quad (1)$$

$$SiO_x + 2xLi^+ + 2xe^- \rightarrow xLi_xO + Si \quad (2)$$

$$SiO_x + xLi^+ + xe^- \rightarrow 0.25xLi_4SiO_4 + (1 - 0.25x)Si \quad (3)$$

Journal Name

ARTICLE

Table 1 The specific capacity (the unit is mAh g^{-1}) and capacity retention ratio of Si@u-SiO_x@GNSs, Si@t-SiO_x@GNSs and Si/GNSs at current densities of 200 mA g^{-1}, 500 mA g^{-1}, 1000 mA g^{-1} and 2000 mA g^{-1}.

	200 mA g^{-1}	500 mA g^{-1}	1000 mA g^{-1}	2000 mA g^{-1}
Si@u-SiO_x@GNSs	1991.3	1673.2 (84.0%)	1296.7 (65.1%)	928.5 (46.6%)
Si@t-SiO_x@GNSs	1200.6	972.9 (81.0%)	702.4 (58.5%)	436.7 (36.4%)
Si/GNSs	617.0	467.0 (75.7%)	315.0 (51.1)	176.9 (28.7%)

$$SiO_x + 0.4xLi^+ + 0.4xe^- \rightleftharpoons 0.2xLi_2Si_2O_5 + (1 - 0.4x)Si \quad (4)$$

Considering about the different percent of GNSs in Si@u-SiO_x@GNSs and Si@t-SiO_x@GNSs, the capacity calculated based on the weight of Si@u-SiO_x and Si@t-SiO_x alone by Equation (5) below are shown in Fig. S3:

$$C_{Si} = (C_{Si-G} - \omega_G \times C_G)/(1 - \omega_G) \quad (5)$$

Where $C_{Si\text{-}G}$ is the measured capacity of Si@u-SiO_x@GNSs or Si@t-SiO_x@GNSs, C_G is the measured capacity of GNSs, ω_G is the percent of GNSs in the composites. It can be calculated that the first discharge capacity of Si@u-SiO_x alone in Si@u-SiO_x@GNSs is as high as 3574.8 mAh g^{-1} which approximate the theoretical capacity of Si at room temperature, and the first reversible capacity is high as 3004.2 mAh g^{-1}. The calculated charge capacity after 50 cycles is 2148.6 mAh g^{-1}, and the calculated reversible capacity of Si@t-SiO_x alone in Si@t-SiO_x@GNSs after 50 cycles is 1178.9 mAh g^{-1} which is much lower than that of the Si@u-SiO_x. All the good electrochemical performance demonstrates that the ultrathin SiO_x shell and good GNSs encapsulation structure can observably improve the reversible capacity and cyclic performance of Si-GNSs composites. To further prove this efficient framework, we also study the influences on cycle performance of Si@u-SiO_x@GNSs by different binders (seeing in the electronic supplementary information). Sodium alginate (SA) has been reported to markedly improve the electrochemical performance of silicon anodes.[42, 44, 64] It shows that cycle performance shown by Si@u-SiO_x@GNSs with SA binder is similar to that with PVDF binder (Fig. S4).

Si@u-SiO_x@GNSs also exhibit good rate capability. As shown in Fig. 5 d and Table 1, the Si@u-SiO_x@GNSs show discharge capacities of 1991.3, 1673.2, 1296.7 and 928.5 mAh g^{-1}, at a current density of 200, 500, 1000 and 2000 mA g^{-1}, respectively. When the current density is back to 200 mA g^{-1}, the discharge capacity can reach to 1740.7 mAh g^{-1}. The capacities of the Si@u-SiO_x@GNSs under different current density are much higher than those of the Si@t-SiO_x@GNSs and Si/GNSs. The capacity retention ratio of the Si@u-SiO_x@GNSs, Si@t-SiO_x@GNSs and Si/GNSs were calculated by C_{cd}/C_{200}, where C_{cd} is the capacity at different current density, C_{200} is the capacity at the current density of 200 mA g^{-1} after first 20 cycles. It is clear to see that the capacity retention ratio of Si@u-SiO_x@GNSs is highest of all, especially under large current density (Table 1). Retention ratio of the Si@t-SiO_x@GNSs is lower than that of Si@u-SiO_x@GNSs for 10.2% even though the GNSs percent of Si@t-SiO_x@GNSs is higher than that in the Si@u-SiO_x@GNSs. To obtain long cycling results, charge/discharge tests at a current density of 2000 mA g^{-1} (200 mA g^{-1} for initial two cycles) were also carried out,

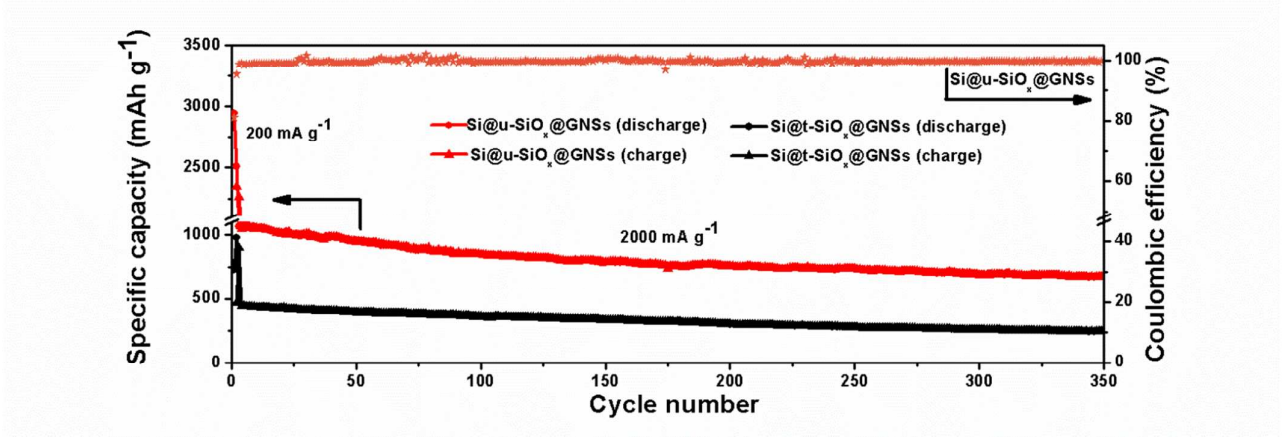

Fig. 6 Long cycle performance of Si@u-SiO_x@GNSs at a current density of 2000 mA g^{-1} (200 mA g^{-1} for initial two cycles).

Journal Name

ARTICLE

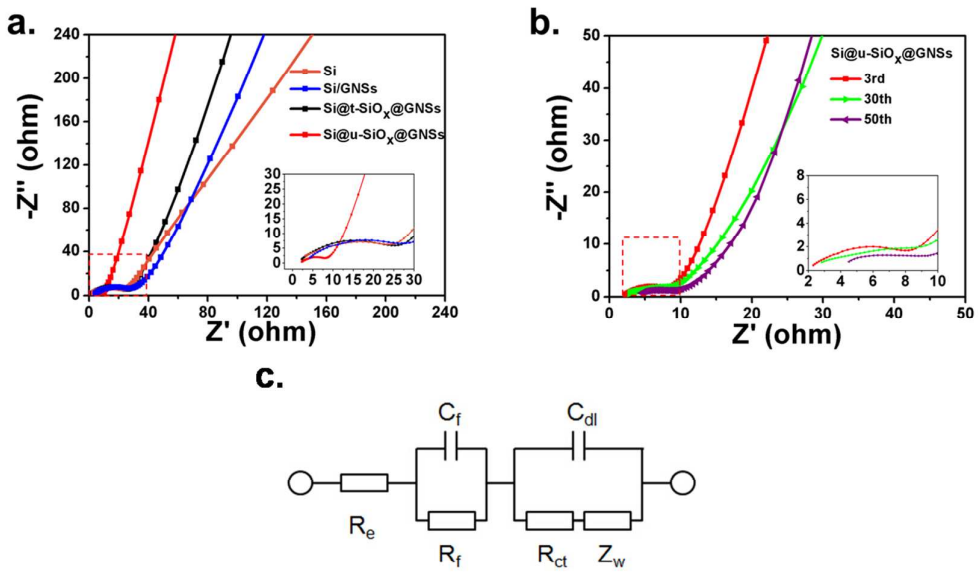

Fig. 7 (a) EIS curves of the Si nanoparticles, Si/GNSs, Si@u-SiO_x@GNSs, and Si@t-SiO_x@GNSs after 3 cycles; (b) EIS curves of the Si@u-SiO_x@GNSs after different cycles; (c) Randles equivalent circuit model of the lithium-ion batteries.

shown in Fig. 6. Even after 350 cycles, reversible capacity of Si@u-SiO_x@GNSs still maintain ~700 mAh g^{-1}, which corresponds 67% of the third charge capacity. But for Si@t-SiOx@GNSs, only 240 mAh g^{-1} is left after 350 cycles (51% of the third charge capacity).

We summarized some typical works in recent years about fabrications and electrochemical performance of Si-GNSs anode materials for LIBs through electrostatic self-assembly method (seeing in the electronic supplementary information, Table S1). It shows that the Si@u-SiO_x@GNSs not only have high 1st charge capacity and reversible capacity after 50 cycles but also a high Coulombic efficiency even though we used PVDF binders which is widely considered not suitable for Si-based anode material. Moreover, the Si@u-SiO_x@GNSs also show excellent rate capability when compared with other Si-GNSs anode materials. What's more, the preparation route presented by us is more efficient and environmental friendly than others.

To investigate the kinetics of the electrochemical process, electrochemical impedance spectroscopy (EIS) were carried out at the cell voltage of 2.0 V. As shown in Fig. 7a and 7b, all the Nyquist plots include two depressed semicircle in the middle and high frequency region, and a sloped line in the low frequency region. The high frequency semicircle is assigned to the SEI film and contact resistance, the middle frequency semicircle can be attributed to the charge-transfer impedance on the interface of the electrolyte and active material, while the linear region corresponds to the lithium ions diffusion in the electrodes.[65, 66] These Nyquist plots were plotted with the equivalent circuit shown in Fig 7c. R_e is the electrolyte impedance, and R_f and C_f are the resistance and capacitance of the SEI layer formed on the surface of the electrodes, respectively. R_{ct} and C_{dl} are the charge-transfer resistance and double-layer capacitance. Z_w is the Warburg impedance related to the diffusion of lithium ions in the electrodes.[67, 68] The simulation results of the kinetic parameters are presented in Table 2.

It can be clearly seen that the R_f value of Si nanoparticles,

Table 2 Simulation results of the kinetic parameters of Si nanoparticles, Si/GNSs, Si@t-SiO_x@GNSs after 3 cycles, and Si@u-SiO_x@GNSs after different cycles.

	R_e (Ω)	R_f (Ω)	R_{ct} (Ω)
Si nanoparticles (3rd)	2.65	6.09	14.80
Si/GNSs (3rd)	4.09	4.84	12.01
Si@t-SiO_x@GNSs (3rd)	2.13	3.97	13.05
Si@u-SiO_x@GNSs (3rd)	2.27	1.26	3.12
Si@u-SiO_x@GNSs (30th)	2.64	1.60	2.13
Si@u-SiO_x@GNSs (50th)	4.33	1.84	2.01

Si/GNSs, Si@t-SiO_x@GNSs and Si@u-SiO_x@GNSs are reduced gradually. This result indicates that GNSs and especially the good encapsulation structure can stabilize the SEI. However, the R_{ct} value of Si@t-SiO_x@GNSs (13.05 Ω) is close to that of Si nanoparticles (14.80 Ω) and is even bigger than that of the Si/GNSs (12.01 Ω). It can be explained by the thick SiO_x increasing the charge-transfer impedance between electrolyte and active material. It worth noting that the R_{ct} value of Si@u-SiO_x@GNSs is low as 3.12 Ω and it reduce slightly to 2.01 Ω after 50 cycles. The good electrochemical activity can be attributed to the ultrathin SiO_x shell and the channel for electrons and lithium ions supplied by GNSs in Si@u-SiO_x@GNSs. The small change of (R_{ct}+ R_f) also demonstrates the more stable SEI formed on the Si@u-SiO_x@GNSs.

4 Conclusions

We presented an environmentally friendly and effective amination method to fabricate GNSs encapsulated Si nanoparticles. NH_2-termitated Si was directly obtained by modifying Si nanoparticles with amino silane in ammonia-water-ethanol solution within a short time. No additional toxic reagents and extra energy are used. Because of ultrathin SiO_x on the Si nanoparticles and good GNSs encapsulation structure, the Si@u-SiO_x@GNSs obtained by self-assembly and thermal reduction exhibit high reversible capacity and show good cycling stability and rate capability.

Acknowledgements

This work was supported by the National Natural Science Foundation of China (51202009 and 51272019), New Teachers' Fund for Doctor Stations, Ministry of Education of China (20120010120004), and Foundation of Excellent Doctoral Dissertation of Beijing City (YB20121001001).

Notes and references

1 A. Dey, *J. Electrochem. Soc.*, 1971, **118**, 1547.
2 C. K. Chan, H. Peng, G. Liu, K. McIlwrath, X. F. Zhang, R. A. Huggins and Y. Cui, *Nat. Nanotechnol.*, 2007, **3**, 31.
3 J. H. Ryu, J. W. Kim, Y.-E. Sung and S. M. Oh, *Electrochem. Solid-State Lett.*, 2004, **7**, A306.
4 Y.-M. Kang, J.-Y. Go, S.-M. Lee and W.-U. Choi, *Electrochem. Commun.*, 2007, **9**, 1276.
5 V. A. Sethuraman, M. J. Chon, M. Shimshak, V. Srinivasan and P. R. Guduru, *J. Power Sources*, 2010, **195**, 5062.
6 Y. M. Lee, J. Y. Lee, H.-T. Shim, J. K. Lee and J.-K. Park, *J. Electrochem. Soc.*, 2007, **154**, A515.
7 B. Key, R. Bhattacharyya, M. Morcrette, V. Seznéc, J.-M. Tarascon and C. P. Grey, *J. Am. Chem. Soc*, 2009, **131**, 9239.
8 H. Wu and Y. Cui, *Nano Today*, 2012, **7**, 414.
9 J. Luo, X. Zhao, J. Wu, H. D. Jang, H. H. Kung and J. Huang, *J Phys. Chem. Lett.*, 2012, **3**, 1824.
10 I. Sandu, P. Moreau, D. Guyomard, T. Brousse and L. Roue, *Solid State Ionics*, 2007, **178**, 1297.
11 H. Kim, M. Seo, M. H. Park and J. Cho, *Angew. Chem. Int. Edit.*, 2010, **49**, 2146.
12 J. Maranchi, A. Hepp and P. Kumta, *Electrochem. Solid-State Lett.*, 2003, **6**, A198.
13 T. Takamura, S. Ohara, M. Uehara, J. Suzuki and K. Sekine, *J. Power Sources*, 2004, **129**, 96.
14 X.-Y. Zhang, L. Zhang, G. Meng, G. Li, N. Jin-Phillipp and F. Phillipp, *Adv. Mater.*, 2001, **13**, 1238.
15 M.-H. Park, M. G. Kim, J. Joo, K. Kim, J. Kim, S. Ahn, Y. Cui and J. Cho, *Nano Lett.*, 2009, **9**, 3844.
16 T. Song, J. Xia, J.-H. Lee, D. H. Lee, M.-S. Kwon, J.-M. Choi, J. Wu, S. K. Doo, H. Chang and W. I. Park, *Nano Lett.*, 2010, **10**, 1710.
17 Y. Yao, M. T. McDowell, I. Ryu, H. Wu, N. Liu, L. Hu, W. D. Nix and Y. Cui, *Nano Lett.*, 2011, **11**, 2949.
18 D. Chen, X. Mei, G. Ji, M. Lu, J. Xie, J. Lu and J. Y. Lee, *Angew. Chem. Int. Edit.*, 2012, **51**, 2409.
19 H. Ma, F. Cheng, J. Y. Chen, J. Z. Zhao, C. S. Li, Z. L. Tao and J. Liang, *Adv. Mater.*, 2007, **19**, 4067.
20 H. Kim, B. Han, J. Choo and J. Cho, *Angew. Chem.*, 2008, **120**, 10305.
21 M. Ge, Y. Lu, P. Ercius, J. Rong, X. Fang, M. Mecklenburg and C. Zhou, *Nano Lett.*, 2013, **14**, 261.
22 L. Shen, X. Guo, X. Fang, Z. Wang and L. Chen, *J. Power Sources*, 2012, **213**, 229.
23 N. Liu, H. Wu, M. T. McDowell, Y. Yao, C. Wang and Y. Cui, *Nano Lett.*, 2012, **12**, 3315.
24 N. Liu, Z. Lu, J. Zhao, M. T. McDowell, H.-W. Lee, W. Zhao and Y. Cui, *Nat. Nanotechnol.*, 2014, **9**, 187.
25 B. Wang, X. Li, X. Zhang, B. Luo, Y. Zhang and L. Zhi, *Adv. Mater.*, 2013, **25**, 3560.
26 D. Shao, D. Tang, Y. Mai and L. Zhang, *J Mater. Chem. A*, 2013, **1**, 15068.
27 S. Park and R. S. Ruoff, *Nat. Nanotechnol.*, 2009, **4**, 217.
28 G. A. Tritsaris, E. Kaxiras, S. Meng and E. Wang, *Nano Lett.*, 2013, **13**, 2258.
29 Y. Zhu, W. Liu, X. Zhang, J. He, J. Chen, Y. Wang and T. Cao, *Langmuir*, 2013, **29**, 744.
30 S. Y. Jeong, S. Yang, S. Jeong, I. J. Kim, H. J. Jeong, J. T. Han, K. J. Baeg and G. W. Lee, *Small*, 2015,**11**, 2274.
31 S.-L. Chou, J.-Z. Wang, M. Choucair, H.-K. Liu, J. A. Stride and S.-X. Dou, *Electrochem. Commun.*, 2010, **12**, 303.
32 J. K. Lee, K. B. Smith, C. M. Hayner and H. H. Kung, *Chem. Commun.*, 2010, **46**, 2025.
33 X. Zhou, Y.-X. Yin, L.-J. Wan and Y.-G. Guo, *Chem. Commun.*, 2012, **48**, 2198.
34 Y. Huang, X.-l. Huang, J.-s. Lian, D. Xu, L.-m. Wang and X.-b. Zhang, *J. Mater. Chem.*, 2012, **22**, 2844.
35 X. l. Huang, R. z. Wang, D. Xu, Z. l. Wang, H. g. Wang, J. j. Xu, Z. Wu, Q. c. Liu, Y. Zhang and X. b. Zhang, *Adv. Funct. Mater.*, 2013, **23**, 4274.
36 M. Yan, F. Wang, C. Han, X. Ma, X. Xu, Q. An, L. Xu, C. Niu, Y. Zhao and X. Tian, *J. Am. Chem. Soc.*, 2013, **135**, 18176.
37 S. Yang, X. Feng, S. Ivanovici and K. Müllen, *Angew. Chem. Int. Edit.*, 2010, **49**, 8408.
38 L. Ma, X. Zhou, L. Xu, X. Xu, L. Zhang and W. Chen, *J. Power Sources*, 2015, **285**, 274.
39 X. Zhou, Y. X. Yin, L. J. Wan and Y. G. Guo, *Adv. Energy Mater.*, 2012, **2**, 1086.
40 H. Tang, J.-P. Tu, X.-Y. Liu, Y.-J. Zhang, S. Huang, W.-Z. Li, X.-L. Wang and C.-D. Gu, *J. Mater. Chem. A*, 2014, **2**, 5834.
41 Z.-F. Li, H. Zhang, Q. Liu, Y. Liu, L. Stanciu and J. Xie, *ACS Appl. Mater. Interfaces*, 2014, **6**, 5996.
42 Y.-S. Ye, X.-L. Xie, J. Rick, F.-C. Chang and B.-J. Hwang, *J. Power Sources*, 2014, **247**, 991.
43 Y. Wen, Y. Zhu, A. Langrock, A. Manivannan, S. H. Ehrman and C. Wang, *Small*, 2013, **9**, 2810.
44 G. Zhao, L. Zhang, Y. Meng, N. Zhang and K. Sun, *J. Power Sources*, 2013, **240**, 212.
45 C. Sun, Y. Deng, L. Wan, X. Qin and G. Chen, *ACS Appl. Mater. Interfaces*, 2014, **6**, 11277.

46 J. Niu, S. Zhang, Y. Niu, R. Song, H. Song, X. Chen, J. Zhou and S. Hong, *RSC Adv.*, 2014, **4**, 29435.
47 T. Suteewong, H. Sai, M. Bradbury, L. A. Estroff, S. M. Gruner and U. Wiesner, *Chem. Mater.*, 2012, **24**, 3895.
48 W. S. Hummers Jr and R. E. Offeman, *J. Am. Chem. Soc.*, 1958, **80**, 1339.
49 S. Zhang, L. Zhu, H. Song, X. Chen, B. Wu, J. Zhou and F. Wang, *J. Mater. Chem.*, 2012, **22**, 22150.
50 D. Krishnan, F. Kim, J. Luo, R. Cruz-Silva, L. J. Cote, H. D. Jang and J. Huang, *Nano Today*, 2012, **7**, 137.
51 H. Bahruji, M. Bowker and P. R. Davies, *Int. J. Hydrogen Energy*, 2009, **34**, 8504.
52 E. T. Vandenberg, L. Bertilsson, B. Liedberg, K. Uvdal, R. Erlandsson, H. Elwing and I. Lundström, *J. Colloid Interface Sci.*, 1991, **147**, 103.
53 M. Obrovac and L. Krause, *J. Electrochem. Soc.*, 2007, **154**, A103.
54 Y. Liu, B. Chen, F. Cao, H. L. Chan, X. Zhao and J. Yuan, *J. Mater. Chem.*, 2011, **21**, 17083.
55 L. Xin, Z. Hailei, X. Jingying, L. Pengpeng, W. Ke and C. Jiajia, *Prog. Chem.* 2015, **27**, 336.
56 B. Guo, J. Shu, Z. Wang, H. Yang, L. Shi, Y. Liu and L. Chen, *Electrochem. Commun.*, 2008, **10**, 1876.
57 P. Lv, H. Zhao, J. Wang, X. Liu, T. Zhang and Q. Xia, *J. Power Sources*, 2013, **237**, 291.
58 Q. Sun, B. Zhang and Z.-W. Fu, *Appl. Surf. Sci.*, 2008, **254**, 3774.
59 W.-S. Chang, C.-M. Park, J.-H. Kim, Y.-U. Kim, G. Jeong and H.-J. Sohn, *Energ. Environ. Sci.*, 2012, **5**, 6895.
60 Y. Nagao, H. Sakaguchi, H. Honda, T. Fukunaga and T. Esaka, *J. Electrochem. Soc.*, 2004, **151**, A1572.
61 M. T. McDowell, S. W. Lee, I. Ryu, H. Wu, W. D. Nix, J. W. Choi and Y. Cui, *Nano Lett.*, 2011, **11**, 4018.
62 L. Su, Z. Zhou and M. Ren, *Chem. Commun.*, 2010, **46**, 2590.
63 S. Sim, P. Oh, S. Park and J. Cho, *Adv. Mater.*, 2013, **25**, 4498.
64 I. Kovalenko, B. Zdyrko, A. Magasinski, B. Hertzberg, Z. Milicev, R. Burtovyy, I. Luzinov and G. Yushin, *Science*, 2011, **334**, 75.
65 R. Song, H. Song, J. Zhou, X. Chen, B. Wu and H. Y. Yang, *J. Mater. Chem.*, 2012, **22**, 12369.
66 S. Yang, H. Song, X. Chen, A. Okotrub and L. Bulusheva, *Electrochim. Acta*, 2007, **52**, 5286.
67 S. Yang, H. Song and X. Chen, *J. Power Sources*, 2007, **173**, 487.
68 S. Zhang, L. Zhu, H. Song, X. Chen and J. Zhou, *Nano Energy*, 2014, **10**, 172.

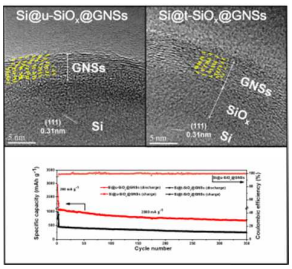

Graphene nanosheets encapsulated Si nanoparticles with ultrathin silica shell have been fabricated by an environmentally friendly and effective amination method.